ACS OMEGA

http://pubs.acs.org/journal/acsodf

Article

Removal of Uranium-238, Thorium-232, and Potassium-40 from Wastewater via Adsorption on Multiwalled Carbon Nanotubes

Saad S. M. Hassan,* Ehab M. Abdel Rahman,* Gehan M. El-Subruiti, Ayman H. Kamel, and Hanan M. Diab

Cite This: *ACS Omega* 2022, 7, 12342−12353

Read Online

ACCESS | Metrics & More | Article Recommendations

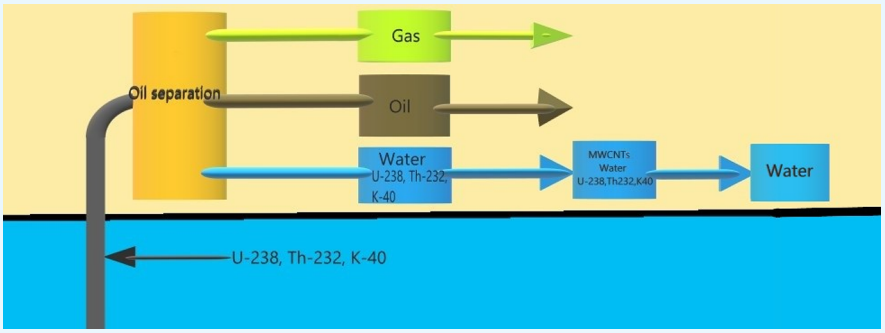

ABSTRACT: The optimum conditions for the removal of uranium-238, thorium-232, and potassium-40 from wastewater and the discharge of nuclear facilities using multiwalled carbon nanotubes (CNTs) are described. The adsorption mechanism is mainly attributed to chemical interactions between the metal ions and surface functional groups of the CNTs. Batch adsorption experiments are carried out in order to study the effect of different parameters such as pH, contact time, initial metal ion concentration, adsorbent dose, and temperatures. Maximum metal removal (>98%) from solutions containing 20−120 Bq/L metal ions is achieved using a contact time of 15 min, a pH of 6.0, and 10 mg/L CNTs. The effect of temperature on the kinetics and equilibrium of adsorption on CNT particles is examined. Consistent with an exothermic reaction, an increase in the temperature resulted in an increase in the adsorption rate. Langmuir, Freundlich, and Dubinin−Radushkevich isotherms are applied to the data obtained at various temperatures. The Langmuir adsorption model is the best for data interpretations. The kinetics of adsorption reveals a pseudo-second-order mechanism. Thermodynamic parameters at 293 K ($\Delta G°$, $\Delta H°$, and $\Delta S°$) for U-238, Th-232, and K-40 are −14590.7 kJ/mol, −6.66 kJ/mol, and 26.47 J/(mol K), −96,96.5 kJ/mol, −2.48 kJ/mol, and 14.17 J/(mol K), and −3922.09 kJ/mol, −1.32 kJ/mol, and 6.12 J/(mol K), respectively.

1. INTRODUCTION

"NORM" refers to a naturally occurring radioactive material that exposes individuals to radiation.[1] Human activities (e.g., burning coal, fertilizer industry, and oil and gas production operations),[2] frequently enhance NORM exposure. One of the main industries with an aqueous TENORM (technologically enhanced NORM) problem is the petroleum industry.[3] The radionuclides identified in oil and gas streams belong to the decay chains of uranium and thorium.[4] When the produced water is brought to the surface, it contains uranium-238, thorium-232, and potassium-40 together with an abundance of other cations, mainly alkaline earth cations.[5] The highly toxic nature of these radioactive metal ions renders the effective separation and removal of these radiotoxic substances from nontoxic compounds highly desirable. These hazardous contaminants are nonbiodegradable and highly toxic and tend to accumulate in living creatures.[6]

The removal of radioactive nuclide ions from wastewater is a crucial step toward improving water quality and ensuring a safe water supply.[7] As a result, it is critical to remove these metal ions from the waste before releasing it into the environment. According to a study by the World Health Organization (WHO), uranium-238, thorium-232, and potassium-40 are some of the most hazardous elements that influence the environment.[8] Several studies have been carried out to identify a suitable and efficient sorbent for the removal of heavy metal ions and other contaminants. Natural inorganic materials, peat,

Received: February 9, 2022
Accepted: March 22, 2022
Published: April 1, 2022

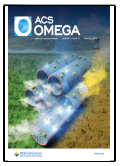

peat moss, algae, yeast biomass, rice husk, nanomaterials, sawdust (SW), and others have been suggested.[9] Carbon multiwalled nanotubes showed promising adsorption efficiency due to their unique structure and properties, especially the large specific surface area and large pore volume.[10,11]

The present work was undertaken to investigate the use of multiwalled carbon nanotubes (MWCNTs) for the removal of uranium-238, thorium-232, and potassium-40 from wastewater. The experimental conditions including the effect of pH, contact time, temperature, and initial concentrations of MWCNTs and the metal ions were optimized, and adsorption mechanisms, thermodynamics, and kinetic models are also discussed.

2. EXPERIMENTAL SECTION

2.1. Chemicals and Equipment. Deionized twice-distilled water was used throughout. All the chemicals are of the highest purity obtained from Sigma-Aldrich. Hydrochloric acid and sodium hydroxide are used for pH adjustment. MWCNTs were prepared via chemical vapor deposition (CVD). In CVD, a volatile precursor undergoes thermal decomposition at elevated temperatures to form a solid deposit on a substrate. The diameter of the tubes ranges between 110 and 170 nm, and the length is between 5 and 9 μm. The multiwalled nanotubes are stable in an inert atmosphere up to a temperature of 3697 °C, according to Sigma-Aldrich production. A Dragon digital hotplate with a magnetic stirrer (MS-H-Pro) and a temperature sensor (PT 1000; IKA) was used. The pH of the test solutions was adjusted using a HANNA HI2211 Ph/ORP meter. A γ-ray spectrometer with a high-purity germanium (HPGe) detector/ORTEC was employed, and point sources of ^{137}Cs (661.6 keV) and ^{60}Co (1172 and 1332.3 keV) were used for the spectrometer energy calibration. Test samples containing NORMs were obtained from the local crude oil company (Suez governorate, Egypt). The half-life for the NORM isotopes is 4.468×10^9 years for uranium-238, 1.4×10^{10} years for thorium-232, and 1.251×10^9 years for potassium-40.

2.2. Methods. Due of the small size of MWCNTs, a batch approach was utilized. These studies were carried out by swirling the MWCNTs with varying concentrations of uranium-238, thorium-232, and potassium-40, and the pH was adjusted to different values ranging from 2 to 8 using hydrochloric acid and/or sodium hydroxide solution. Adsorption experiments were conducted at various contact times (5, 10, and 15 min), temperatures (293, 303, and 313 K), and MWCNT dosages (0.004, 0.008, and 0.01 g). All figures representing the experimental data were based on the average of triplicate runs. The standard deviation did not exceed ±3%. The initial uranium-238, thorium-232, and potassium-40 ion concentrations were 27.9, 55.8, and 111.6 Bq/L for uranium-238, 5.91, 11.83, and 23.67 for thorium-232, and 19.3, 38.61, and 77.22 Bq/L for potassium-40 for MWCNT dosages of 0.004, 0.008, and 0.01 g, respectively. Aliquots of the test sample solutions were collected at regular intervals, filtered to remove particulates, and examined using a γ-ray spectrometer with an HPGe detector. The concentrations of the metal ions before and after adsorption were measured. The data were used to compute q_e (mg/g), which is the difference between the initial and equilibrium metal concentrations, and q_t (mg/g), which is the difference between the initial and temporal variations (t) of metal concentrations (eqs 1 and 2, respectively)

$$q_e = \frac{(C_o - C_e)V}{m} \quad (1)$$

$$q_t = \frac{(C_o - C_t)V}{m} \quad (2)$$

Metal removal (%) was determined using eq 3

$$\% \text{ removal} = \frac{C_o - C_t}{C_o} \times 100 \quad (3)$$

where C_o (mg/L) is the initial metal concentration, C_e (mg/L) is the equilibrium concentration of the metal ions, C_t (mg/L) is the metal concentration in the solution after time t, m (g) is the used mass of the MWCNT dose, and V is the volume of the test solution represented by C_t (mg/L).

2.3. Adsorption Kinetics Modeling. The kinetics of the metal removal was studied using a series of solutions having various initial concentrations of uranium-238, thorium-232, and potassium40 ions. Batch adsorption experiments were also conducted with various pH values, contact durations, dosages, metal concentrations, and temperature parameters. Applicability of pseudo-first-order, pseudo-second-order, and kinetic models was tested under the experimental conditions. Different aliquots of uranium-238, thorium-232, and potassium-40 ions were subjected to batch adsorption experiments using a stirring rate of 600 rpm and a 0.01 g MWCNT dosage at 293 K. The data were used to test the applicability of the adsorption isotherms of Langmuir, Freundlich, and Dubinin−Radushkevich (D−R).

2.4. Effect of Initial Metal Concentrations. A 0.01 g portion of the adsorbents (MWCNTs) was added to solutions containing 111.6, 23.67, and 77.2 Bq/L of uranium-238, thorium-232, and potassium-40, respectively. The mixtures were stirred using a magnetic stirrer for 15 min at 600 rpm. After different intervals of time (5, 10, and 15 min), the solutions were filtered off through Whatman no. 1 filter paper. The metal ions were quantified using the HPGe detector-based γ-ray spectrometer. The experiment was repeated using different doses of the adsorbent (MWCNTs).

2.5. Effect of pH of the Test Solutions. To 20 mL aliquots of uranium-238, thorium-232, and potassium-40 solutions, 0.01 g of the MWCNT adsorbents was added. The pH of the solutions was adjusted to 2, 4, 6, and 8 by adding 1.0 N HCl and/or NaOH. Using a 600 rpm mixer, the mixture was stirred, and the remaining concentrations were measured after 5, 10, and 15 min intervals using a HPGe detector-based γ-ray spectrometer.

2.6. Effect of Contact Time. Different portions (0.004, 0.008, and 0.01 g) of the MWCNT adsorbent were added to aqueous solutions containing uranium-238, thorium-232, and potassium-40. The solutions were stirred at 600 rpm, and the metal contents were measured at time intervals of 5, 10, and 15 min.

2.7. Effect of Temperature. Adsorbents (MWCNTs) were added to uranium-238, thorium-232, and potassium-40 test solutions with the concentrations of 27.9, 55.8, and 111.6, Bq/L for uranium-238, 5.91, 11.83, and 23.67 Bq/L for thorium-232, and 19.3, 38.61, and 77.2 Bq/L for potassium-40, respectively. The temperature of the solutions was adjusted to 293, 303, and 313 K, and the solution was stirred at a rate of 600 rpm. The solutions were filtered off, and the remaining metal ions were measured using the HPGe detector-based γ-ray spectrometer at time intervals of 5, 10, and 15 min. The

https://doi.org/10.1021/acsomega.2c00819
ACS Omega 2022, 7, 12342−12353

experiment was repeated at different temperatures T = 293, 303, and 313 K.

3. RESULTS AND DISCUSSION

Several factors affecting the reaction rate and influencing the removal of uranium-238, thorium-232, and potassium-40 nuclides from wastewater using MWCNTs have been investigated and optimized.

3.1. Effect of pH. The influence of pH on metal sorption was investigated because variation of solution acidity affects the ionization state of the sorbent functional groups. Equilibrium experiments were conducted with initial uranium-238, thorium-232, and potassium-40 test solutions with concentrations of 111.6, 23.67, and 77.22 Bq/L, respectively. The pH ranged from 2.0 to 8.0. To adjust the pH of the metal ions, a dilute NaOH and/or HCl solution was added to the test solution. Increasing the pH slightly increases metal sorption to reach a maximum adsorbing capacity at a pH of 6.0 and then decrease, as shown in Figures 1 and 2. While uranium-238 and

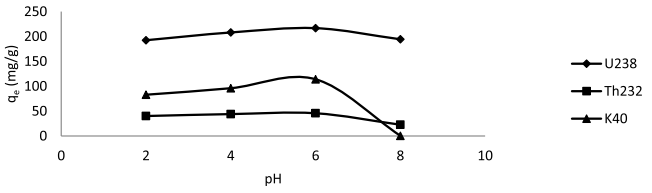

Figure 1. Effect of pH on q_e (mg/g) due to adsorption of uranium-238, thorium-232, and potassium-40 onto MWCNTs (initial metal concentration = 111.6, 23.67, and 77.22 Bq/L, respectively, MWCNT dose = 0.01 g, stirring speed = 600 rpm, T = 293 K, and contact time = 15 min).

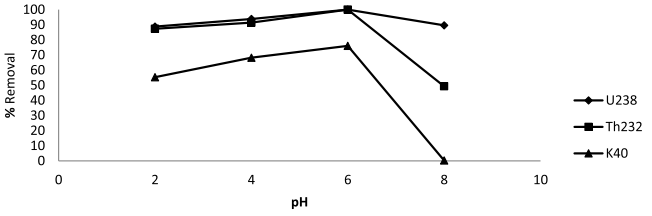

Figure 2. Effect of pH for on adsorption of uranium-238, thorium-232, and potassium40 onto MWCNTs (the initial concentration = 111.6 23.67, and 77.22 Bq/L, respectively, MWCNT dose = 0.01 g, stirring speed = 600 rpm, T = 293 K, and contact time = 15 min).

thorium-232 ions are removed more efficiently at a pH of 2.0 than at a pH of 8.0, potassium-40 ions are not. Despite the fact that metal removal is more effective in acidic environments, a mild adsorption slightly occurs under some acidic circumstances. Under these conditions, the bulk of the functional component groups on the adsorbent are protonated, leaving a few ionizing groups free and available for the adsorption process.[12] This explains the weak metal ion adsorption in an acidic medium due to competition between protons and metal cation species.[13] The high adsorption at high pH values may be attributed to the presence of free lone pair of electrons on the adsorbate, suitable for coordination with the metal ions. The metal ions are generally solved and hydrolyzed in an aqueous solution.[14]

It can be seen that increasing the pH up to 6 is associated to a slight increase of the adsorption effectiveness and the percentage removal of the metal ions due to the replacement of the hydrogen ions on the surface of carbon nanotubes by the metal ions.[15]

3.2. Effect of Contact Time. Data from several measurements conducted at different contact times between the metal ions and MWCNTs were averaged, and the adsorption of metal ions was plotted as a function of time. A period of 15 min was sufficient to almost quantitatively remove all metal ions from the test solutions (Figures 4, 6, and 8). In order to

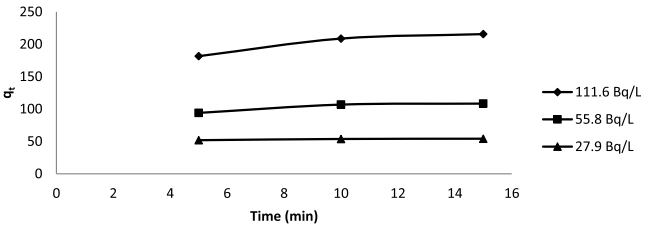

Figure 3. Relationship between q_t (mg/g) and time at different concentrations of uranium-238 on 0.01 g of MWCNTs at 600 rpm and 293 K.

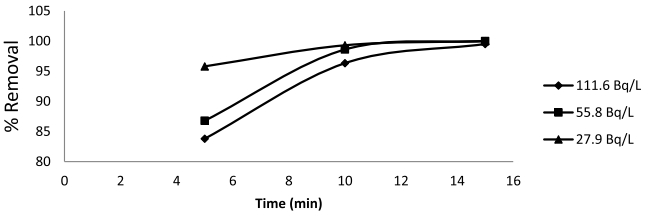

Figure 4. Effect of contact time on the adsorption of uranium-238 onto MWCNTs (initial metal concentrations = 27.9, 55.8, and 111.6 Bq/L, MWCNT dose = 0.01 g/L, pH = 6, stirring speed = 600 rpm, contact time 15 min, and T = 293 K).

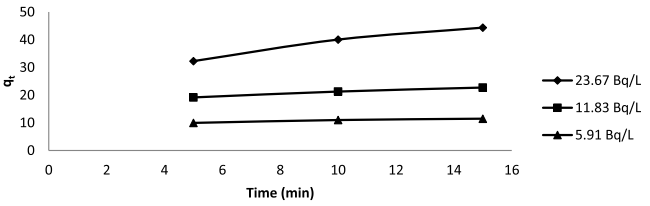

Figure 5. Relationship between q_t (mg/g) and time at different concentrations of thorium-232 on MWCNTs at 600 rpm and 293 K, with 0.01 g of MWCNTs.

determine the adsorption efficiency, three different initial metal concentrations and 0.01 g/L MWCNTs were used to measure the metal concentration change in the aqueous solutions before and after the adsorption equilibrium. Because the

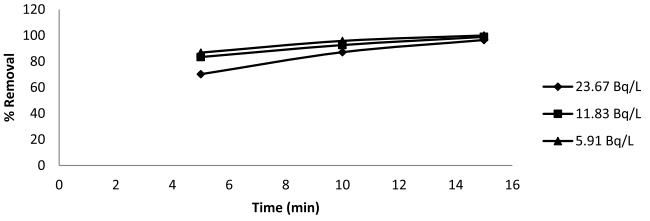

Figure 6. Effect of contact time for adsorption of thorium-232 onto MWCNTs (the initial concentration = 5.91, 11.83, and 23.67 Bq/L, MWCNT dose = 0.01 g/L, pH = 6, stirring speed = 600 rpm, contact time = 15 min, and T = 293 K).

https://doi.org/10.1021/acsomega.2c00819
ACS Omega 2022, 7, 12342−12353

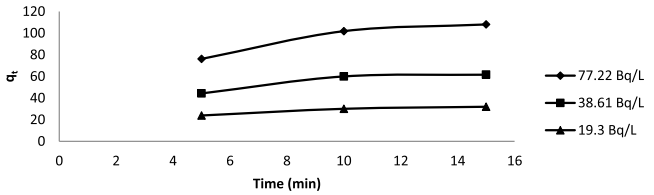

Figure 7. Relationship between q_t (mg/g) and time at different concentrations of potassium-40 at 600 rpmand 293 K with 0.01 g of MWCNTs.

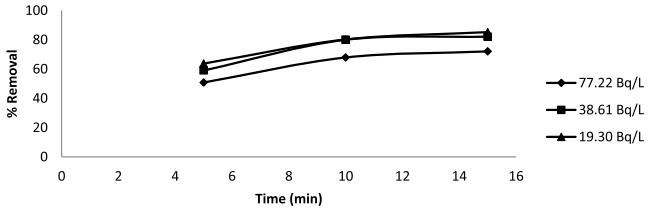

Figure 8. Effect of contact time for adsorption of potassium-40 onto MWCNTs (the metal concentrations = 77.22, 38.61, and 19.30 Bq/L, carbon nanotube dose = 0.01 g/l, pH = 6.0, stirring speed = 600 rpm, contact time = 15 min, and T = 293 K).

adsorption capacity remained virtually constant for all quantities of metal and carbon nanotubes tested, it was deemed to represent the equilibrium state. There was a possibility that the initial speed was related to the surface adsorption, wherein the adsorbent surface is free. A higher rate of reaction occurred next, followed by the adsorbed metals penetrating and adhering to the porous adsorbents (intraparticle diffusion).[16] Both the sorption process and the adsorption equilibrium began to open up a large number of pores, as seen in Figures 3, 5, and 7. Uranium-238, thorium-232, and potassium-40 have different initial metal ion concentrations; with uranium-238 averaging 111.6 Bq/L and thorium-232 averaging 23.67 Bq/L. From these plots, it was clear that the amount of metal adsorption significantly increased with the increasing contact time at all initial metal concentrations, reaching a state of equilibrium within 15 min.[17]

These results revealed a noticeable increase of q_t (mg/g) with the increase of the initial metal ion concentration. In these set of kinetic experiments, uranium-238 and potassium-40 metal ions were rapidly adsorbed on the outer surface of MWCNTs, followed by a sluggish intraparticle diffusion in the interior adsorbent pores. Accordingly, these two-stage metal ion uptakes simultaneously occur on the binding sites of two distinct adsorbent particle types (Figure 9).[18]

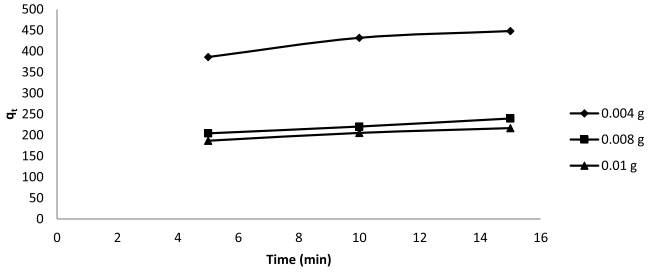

Figure 9. Relation between q_t and time at different doses of carbon nanotubes at 600 rpm and 293 K with 111.6 Bq/L initial uranium-238 concentration.

3.3. Effect of the Adsorbent Dose. The dose of an adsorbent determines the capacity of an adsorbent for a certain initial concentration of the metal adsorbate. While maintaining other parameters constant (i.e., pH; stirring speed; temperature; initial uranium-238, thorium-232, and potassium-40 ion concentrations; and contact time), the dependence of uranium-238, thorium-232, and potassium-40 adsorption on different doses of the MWCNT adsorbent (0.004, 0.008, and 0.01 g) was examined. According to Figures 10−14, the removal % of uranium-238, thorium-232, and potassium-40 ions was increased by increasing the adsorbent dosage of MWCNTs from 0.004 to 0.01 g.

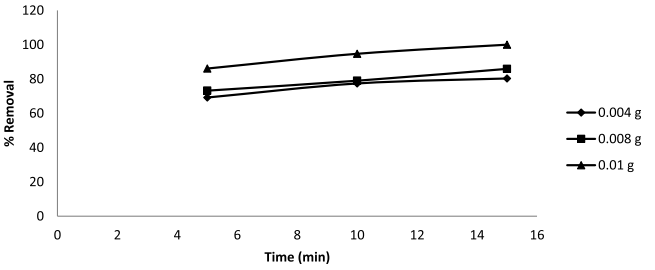

Figure 10. Relation between % removal and time at different doses of carbon nanotubes at 600 rpm, 293 K, and an initial concentration of 111.6 Bq/L of uranium-238.

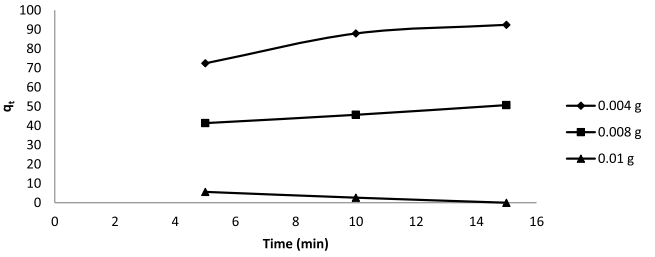

Figure 11. Relation between q_t and time at different doses of MWCNTs at 600 rpm and 293 K with a 23.67 Bq/L initial concentration of thorium-232.

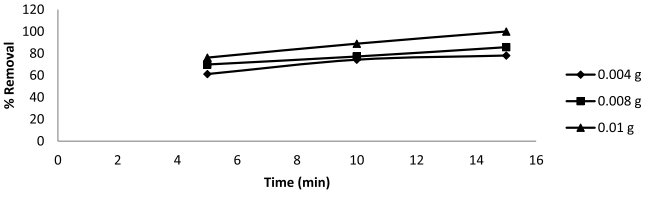

Figure 12. Relation between % removal and contact time at different doses of carbon nanotubes at 600 rpm, 293 K, and an initial concentration of 23.67 Bq/L of thorium-232.

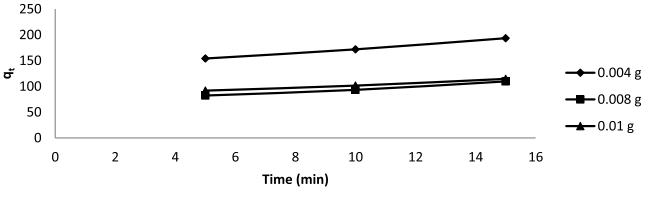

Figure 13. Relation between q_t and time at different doses of MWCNTs at 600 rpm, 293 K, and an initial concentration of 77.22 Bq/L of potassium-40.

https://doi.org/10.1021/acsomega.2c00819
ACS Omega 2022, 7, 12342−12353

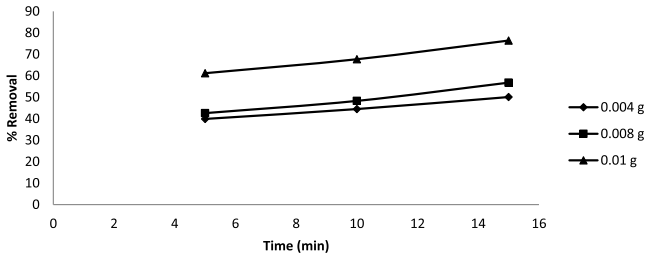

Figure 14. Relation between % removal and contact time at different doses of MWCNTs at 600 rpm, 293 K, and an initial concentration of 77.22 Bq/L of potassium-40.

3.4. Effect of the Initial Metal Ion Concentration. Metal ion adsorption was significantly influenced by its initial concentration in the test solutions. The removal % of uranium-238, thorium-232, and potassium-40 decreased from 100 to 99.5% with the increase of the initial metal ion concentrations from 27.9 to 111.6 Bq/L. At lower metal ion concentrations, the ratio of the initial concentration of uranium-238, thorium-232, and potassium-40 to the available adsorption sites was low; thus, complete adsorption occurred. However, at higher metal ion concentrations, the available adsorption sites decreased compared to the concentration of the metal ions present in the solution due to the lack of sufficient active sites on MWCNTs, and thus, the percentage sorption of metals decreased.[19] The amount of metal ions, q_e (mg/g), increased with the increasing initial metal concentration, as shown in Figures 15–17.

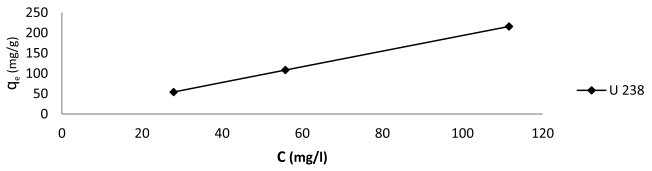

Figure 15. Relation between q_e and initial concentration of uranium-238.

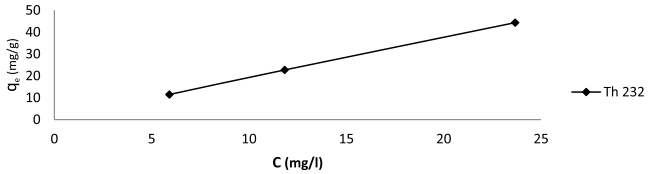

Figure 16. Relation between q_e and initial concentration of thorium-232.

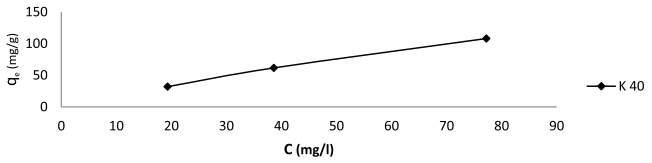

Figure 17. Relation between q_e and initial concentration of potassium-40.

3.5. Effect of Temperature. The temperature has a significant impact on the adsorption mechanism. Adsorption is increased when temperature is increased because it decreases viscosity and therefore speeds up the passage of adsorbed molecules through the adsorbent's exterior boundary layer.[20] Batch adsorption tests were conducted at temperatures of 293, 303, and 313 K, and the results are presented in Figures 18–20. Uranium-238 and potassium-40 ions become more

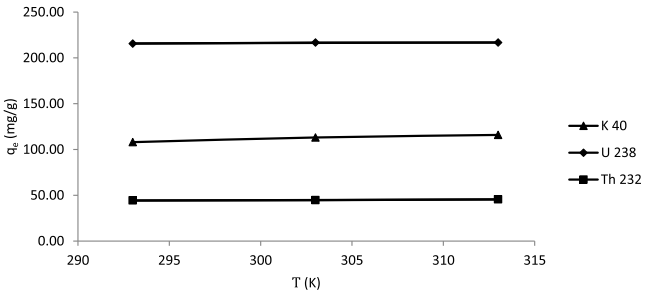

Figure 18. Relation between temperature and different initial metal concentrations (111.6, 23.67, and 77.22 Bq/L, respectively) of uranium-238, thorium-232, and potassium-40 mg/g at a 0.01 g/L dose of MWCNTs and 600 rpm.

mobile when the temperature increases because the retarding forces acting on them are reduced. As a result, the adsorbent's sorption capacity is increased, the chemical interaction between the adsorbate and adsorbent is also increased, and more surface active centers are generated. At higher temperatures, an increased rate of intraparticle diffusion of the metal

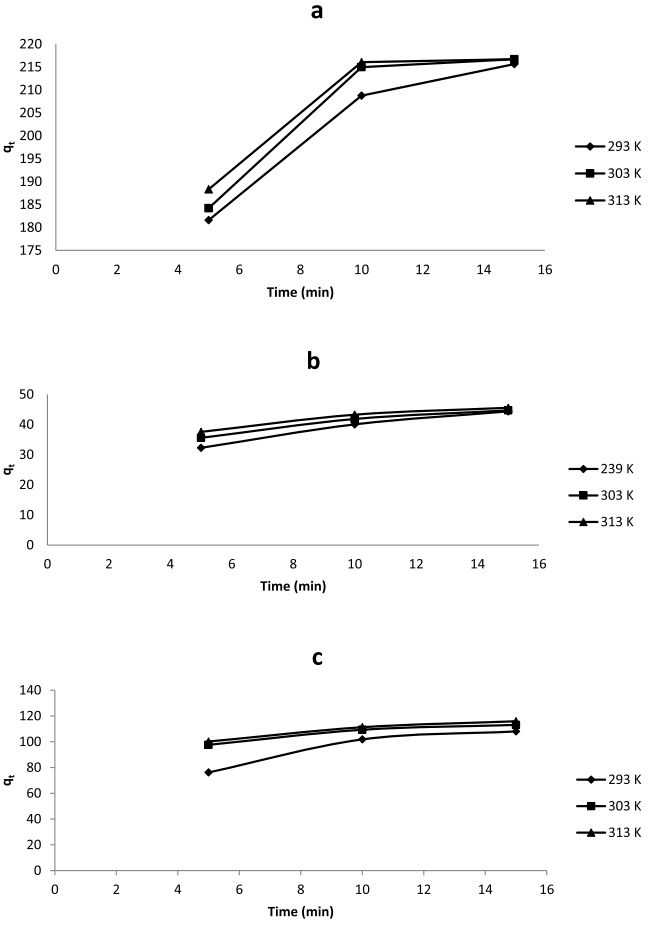

Figure 19. Relationship between q_t and time at different temperatures, initial metal ion concentrations of 111.6, 23.67, and 77.22 Bq/L, a 0.01 g/L dose of MWCNTs, and 600 rpm. (a) Uranium-238; (b) thorium-232; and (c) potassium-40.

https://doi.org/10.1021/acsomega.2c00819
ACS Omega 2022, 7, 12342−12353

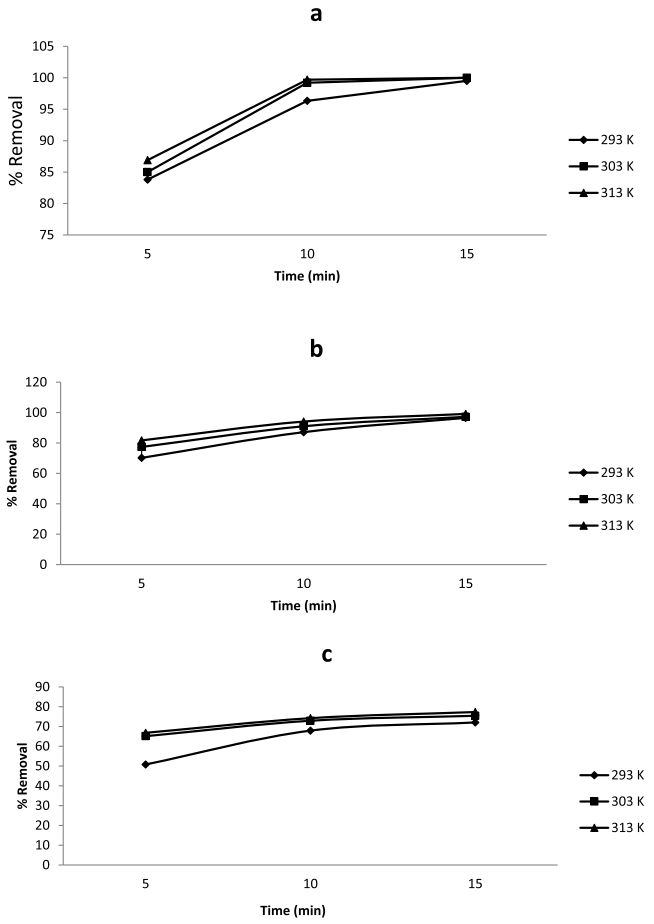

Figure 20. Relationship between % metal ion removal and time at different temperatures, at initial concentrations of 111.6, 23.67, and 77.22 Bq/L, a 0.01 g/L dose of MWCNTs, and 600 rpm. (a) Uranium-238; (b) thorium-232; and (c) potassium-40.

ions into the pores of the adsorbent may be considered.[21] These point to a possible exothermic adsorption process.[21,22] The temperature dependency of the adsorption technique is related to the changes of several thermodynamic factors. Using the obtained adsorption equilibrium data for various temperatures, significant thermodynamic characteristics such as standard Gibbs free energy (ΔG°), standard enthalpy change (ΔH°), and standard entropy change (ΔS°) are computed. These parameters were estimated using eqs 4−7

$$K_e = \frac{q_e}{C_e} \tag{4}$$

$$\Delta G^\circ = -RT \ln K_e \tag{5}$$

$$\Delta G^\circ = \Delta H^\circ - T\Delta S^\circ \tag{6}$$

$$\ln K_e = \frac{\Delta S^\circ}{R} - \frac{\Delta H^\circ}{RT} \tag{7}$$

where q_e is the equilibrium concentration of uranium-238, thorium-232, and potassium-40 ions adsorbed onto the MWCNT from the solution, C_e is the equilibrium concentration of uranium-238, thorium-232, and potassium-40 in the solution, R is the gas constant, T is the absolute temperature, and K_e is the adsorption equilibrium constant.

A van't Hoff plot of $\ln(K_e)$ against $1/T$ was constructed and used to determine ΔH° and ΔS°. The values of ΔG°, ΔH°, and ΔS° are presented in Table 1. A reduction in Gibbs free energy of uranium-238 and potassium-40 adsorption onto

Table 1. Thermodynamic Parameters of Uranium-238, Thorium-232, and Potassium-40 Ions onto MWCNTs at Constant Initial Concentrations

		thermodynamic parameters		
radioactive nuclides	T (K)	ΔG° (kJ/mol)	ΔH° (kJ/mol)	ΔS° (J/mol K)
uranium-238	293	−14590.70		
	303	−13842.80	−6.65	26.47
	313	−16881.46		
thorium-232	293	−9696.04		
	303	−10607.21	−2.48	14.17
	313	−13961.59		
potassium-40	293	−3922.09		
	303	−4494.24	−1.32	6.12
	313	−4915.38		

MWCNTs was found as the temperature increased, and its values were negative at all temperatures examined in the present work. Adsorption of uranium-238, thorium-232, and potassium-40 is an exothermic reaction, as confirmed by the negative Gibbs' free energy (ΔH°). Adsorption rates and capacities are high at high temperatures, enabling metal ions to be rapidly adsorbed.[23] When adsorption of radionuclide ions occurs, the enhanced unpredictability at the solid/liquid interface allows for randomness to prevail in the system,[24] as can be seen in Figure 14. Uranium-238 ions, thorium-232 ions, and potassium-40 ions are all adsorbed more easily as the temperature increases, suggesting an exothermic adsorption process, which may be ascribed to an increase in ion mobility. This increases the quantity of ions that interact with the active sites on adsorbent surfaces. In aqueous-phase adsorption, other studies have discovered similar patterns. This means that, as indicated in eq 1, the sign of ΔG° depends on the entropy term ΔS° (eq 6). It is important to note, as well, that the negative values of ΔG° are indicative of the spontaneous adsorption behavior. Temperature-dependent ΔG° values demonstrate that higher temperatures promote greater spontaneous reactions. As a result, the entire adsorption process of the tested radionuclides may be attributed to intraparticle diffusion (Figure 21).

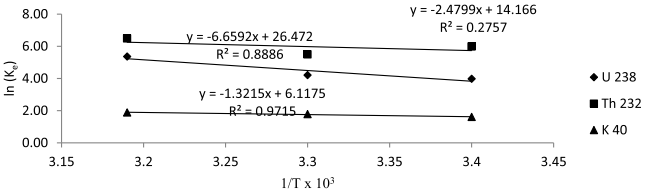

Figure 21. Relationship between $\ln(K_e)$ and reciprocal of temperature at initial concentrations of 111.6, 23.67, and 77.22 Bq/L for uranium-238, thorium-232, and potassium-40, respectively, a 0.01 g/L dose of MWCNTs, and 600 rpm.

3.6. Adsorption Kinetics. In order to understand the nature of adsorption processes, evaluation of the efficacy of adsorbents for the tested metal ions is undertaken by using kinetic models and choosing the optimal operating parameters for the full-scale batch process. This requires knowledge of the dynamics of uranium-238, thorium-232, and potassium-40 to

https://doi.org/10.1021/acsomega.2c00819
ACS Omega 2022, 7, 12342−12353

develop and simulate adsorption processes. This was achieved by examining the pseudo-first-order models,[25] as well as the pseudo-second-order models. Experimental findings and model-predicted values were compared using correlation coefficients (R^2, values close or equal to the value 1, the relatively higher value is the more applicable model). Figures 3, 5, and 7 show the removal of uranium-238, thorium-232, and potassium-40 via adsorption as a function of contact time. MWCNTs display good removal % over the first 15 min. There was no increase in adsorption when the contact period exceeded 15 min. According to these observations, the metal ion adsorption to the adsorbent occurred quite quickly. As part of the investigation of the process of adsorption and its probable rate-controlling measures, which entail mass movement and chemical reaction prowess, two kinetic models are employed to evaluate the experimental results. Kinetic data are well-correlated to describe how metal ions are adsorbed in the solid phase. A summary of kinetic parameters is shown in Table 2. For each model, the R^2 values are compared in order to assess the model validity. The data displayed in Table 2 agree fairly well with the pseudo-second order model.

3.7. Kinetic Model (Pseudo-First-Order). The oldest known equation for the adsorption rate as a function of the adsorption capacity is Lagergren's pseudo-first-order model (eq 8)

$$\ln(q_e - q_t) = \ln(q_e) - k_1 t \tag{8}$$

where k_1, q_e (mg/g), and q_t (mg/g) are the metal quantities adsorbed per unit mass at the equilibrium at any time. Figures 22−24 and Table 2 display the values of k_1 and q_e. The true test of the validity of eq 8 is a comparison of the empirically measured q_e values with those derived from plots of $\ln(q_e - q_t)$ versus t.[25,26] The correlation coefficients for the pseudo-first-order kinetic model are low, and a difference in the equilibrium adsorption capacity (q_e) between the experimental data and the calculated data was observed, indicating a poor pseudo-first-order fit to the experimental data.

3.8. Kinetic Model (Pseudo-Second-Order). The kinetic data are based on the assumption that the adsorption process follows a pseudo-second-order model (eq 9).

$$\frac{t}{q_t} = \frac{1}{k_2 q_e^2} + \frac{1}{q_e} t \tag{9}$$

where k_2 is the pseudo-second-order rate constant for adsorption (mg g^{-1} min^{-1}). As shown in Figures 18 and 19, the slope and intercept may be used to obtain q_e (q_e = 1/intercept) and K_2 [k_2 = (slope)^2/intercept] values from the linear plots given in Figures 25−27. For each of the aforementioned two models, presented in the figures, a linear plot was employed to test their applicability. In order to assess the applicability of each model, the correlation coefficient, R^2, was computed from these plots. Table 1 shows that the kinetic rate constants obtained from the first- and second-order pseudo-kinetic models. The pseudo-second-order adsorption model's correlation coefficient, R^2, is relatively high (>0.9979), and the adsorption capacities calculated by the model are also close to those determined from the experiments. The R^2 values for the pseudo-first-order model, on the other hand, are not satisfactory.[27] As a result, the pseudo-second-order adsorption model was found to be more suitable for describing uranium-238, thorium-232, and potassium-40 adsorption kinetics on MWCNTs.

Table 2. Kinetic Models and Related Parameters for Adsorption of (a) Uranium-238; (b) Thorium-232; and (c) Potassium-40 onto a 0.01 g Dose of MWCNTs at Different Initial Concentrations of Metal Ions, 600 rpm, and 293 °C

(a)		concentration of uranium-238		
kinetic models	parameters	111.6 (Bq/L)	55.80 (Bq/L)	27.90 (Bq/L)
pseudo-first-order equation	q_e (exp) (mg/g)	215.64	108.3	54.175
	q_e (calc.) (mg/g)	4.29	2.77	0.36
	k_1 (min^{-1})	−0.44	−0.31	−0.07
	R^2	0.99	0.75	0.11
pseudo-second-order equation	q_e (calc.) (mg/g)	238.10	117.65	55.25
	k_2 (g/mg min)	0.003	0.01	5.65×10^{-2}
	$k_2 q_e^2$ (mg/g min)			
	$k_2 q_e^2$			
	$t_{0.5}$			
	R^2	1.0	1.0	1.0
(b)		concentration of thorium-232		
kinetic models	parameters	23.67 (Bq/L)	11.83 (Bq/L)	5.91 (Bq/L)
pseudo-first-order equation	q_e (exp) (mg/g)	44.35	22.72	11.47
	q_e (calc.) (mg/g)	3.81	1.812	0.31
	k_1 (min^{-1})	−0.25	−0.13	−0.04
	R^2	0.99	0.95	0.13
pseudo-second-order equation	q_e (calc.) (mg/g)	27.32	12.52	6.21
	k_2 (g/mg min)	0.01	0.05	0.13
	$k_2 q_e^2$ (mg/g min)			
	$k_2 q_e^2$			
	$t_{0.5}$			
	R^2	1.0	1.0	1.0
(c)		concentration of potassium-40		
kinetic models	parameters	77.22 (Bq/L)	38.61 (Bq/L)	19.30 (Bq/L)
pseudo-first-order equation	q_e (exp) (mg/g)	108.02	61.67	31.94
	q_e (calc.) (mg/g)	5.22	3.96	2.99
	k_1 (min^{-1})	−0.35	−0.29	−0.21
	R^2	1.0	0.87	0.95
pseudo-second-order equation	q_e (calc.) (mg/g)	136.99	76.34	38.46
	k_2 (g/mg min)	0.002	0.004	0.009
	$k_2 q_e^2$ (mg/g min)			
	$k_2 q_e^2$			
	$t_{0.5}$			
	R^2	1.0	0.99	1.0

In general, the adsorption process proceeds in three steps: (i) the adsorbate moves from the bulk solution to an adsorbent surface via diffusion; (ii) the adsorbate migrates into adsorbent

https://doi.org/10.1021/acsomega.2c00819
ACS Omega 2022, 7, 12342−12353

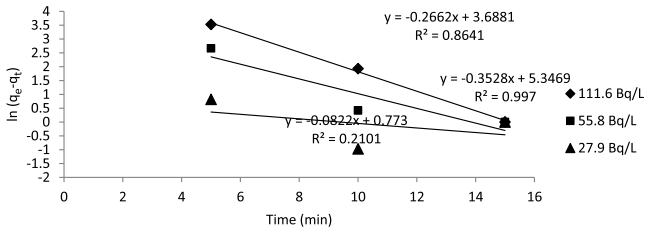

Figure 22. Pseudo-first-order kinetic model for the adsorption of uranium-238 ions onto MWCNTs at different initial metal concentrations, a 0.01 g MWCNT dose, 600 rpm, and 293 K.

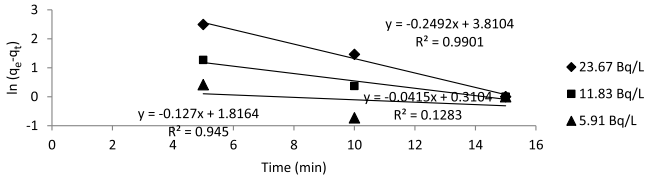

Figure 23. Pseudo-first-order kinetic model for the adsorption of thorium-232 ions onto MWCNTs at different initial metal concentrations, a 0.01 g MWCNT dose, 600 rpm, and 293 K.

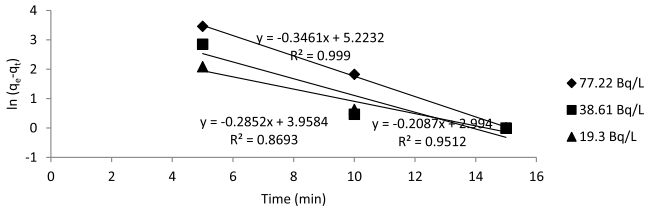

Figure 24. Pseudo-first-order kinetic model for the adsorption of potassium-40 ions onto carbon nanotubes at different initial metal concentrations, a 0.01 g MWCNT dose, 600 rpm, and 293 K.

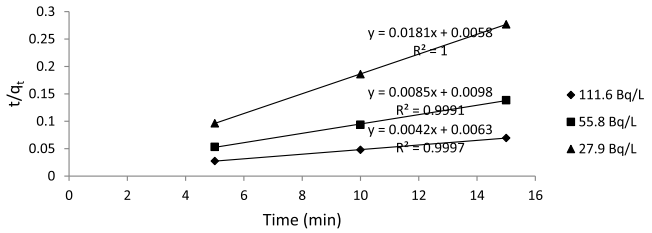

Figure 25. Pseudo-second-order kinetic model for the adsorption of uranium-238 onto MWCNTs at different initial metal concentrations, a 0.01 g MWCNT dose, 600 rpm, and 293 K.

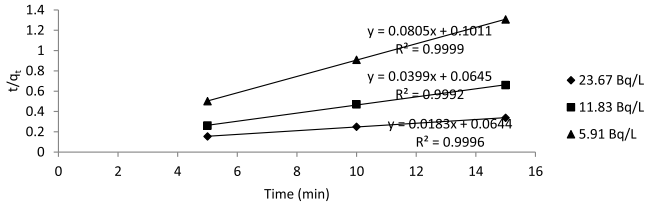

Figure 26. Pseudo-second-order kinetic model for the adsorption of thorium-232 ions onto MWCNTs at different initial metal concentrations, a 0.01 g MWCNT dose, 600 rpm, and 293 K.

pores; and (iii) the adsorbate interacts with the accessible sites on the inner surface of pores.[28]

3.9. Equilibrium Adsorption Study. Adsorption process design and optimization necessitate the establishment of an adequate isotherm model. Some of the established isotherm

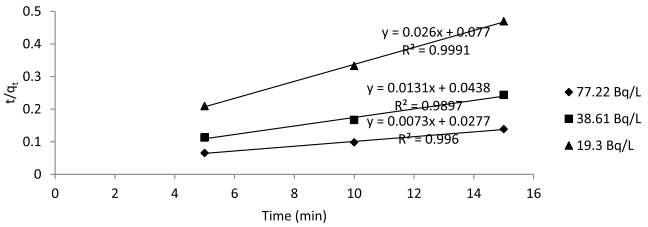

Figure 27. Pseudo-second-order kinetic model for the adsorption of potassium-40 ions onto MWCNTs at different initial metal concentrations, a 0.01 g MWCNT dose, 600 rpm, and 293 K.

models for estimating the equilibrium adsorption of chemicals from solutions are known; these are Langmuir, Freundlich, Redlich−Peterson, D−R, Sips, and Temkin. Because the Langmuir, Freundlich, and D−R equations are the most often employed to analyze the adsorption isotherm, the experimental data of this work were fit using these three models. Equilibrium adsorption isotherms are useful for assessing metal ion adsorption capacity as well as identifying the type of adsorption on MWCNTs.[28,29]

3.10. Langmuir Model. The theoretical Langmuir sorption isotherm[28] is often used to represent the adsorption of a solute from a liquid solution as monolayer adsorption on a surface with a limited number of identical sites. The Langmuir isotherm model assumes homogeneous surface adsorption energies with no adsorbate transmigration in the plane of the surface. The Langmuir isotherm model was next examined to estimate the maximum adsorption capacity corresponding to the full monolayer coverage on the sorbent surface. The Langmuir isotherm model's linear representation is expressed in eq 10.[30]

$$\frac{C_e}{q_e} = \frac{1}{q_{max} b} + \frac{C_e}{q_{max}} \tag{10}$$

In this equation, q_e is equal to the equilibrium metal ion concentration of the adsorbent in milligrams per gram, C_e is equal to the equilibrium metal ion concentration of the solution, q_{max} is equal to the monolayer adsorption saturation capacity of the adsorbent, and b is equal to the Langmuir constant. Using a regression equation, the Langmuir isotherm parameters were calculated, as shown in Figure 28, and the results are summarized in Table 3. In order to determine b and q_{max}, the slope and intercept of the plots were employed. Langmuir's adsorption model performs exceptionally well with metal ions, as seen by high R^2 values.

In addition, the Langmuir isotherm can be expressed in terms of a dimensionless constant separation factor (R_L), which is defined in eq 11

$$R_L = \frac{1}{1 + bC_o} \tag{11}$$

where C_o is the initial concentration of the metal ion and the values of R_L indicate the type of isotherm to be either unfavorable ($R_L > 1$), linear ($R_L = 1$), favorable ($0 < R_L < 1$), or irreversible ($R_L = 0$). The present study shows R_L values in the range of 0.66−0.88, 0.06−0.88, and 0.68−0.88 for uranium-238, thorium-232, and potassium-40, respectively. These data indicate that the adsorption process is more favorable.[29,30]

3.11. Freundlich Model. According to the Freundlich isotherm model, which is commonly used in the case of

https://doi.org/10.1021/acsomega.2c00819
ACS Omega 2022, 7, 12342−12353

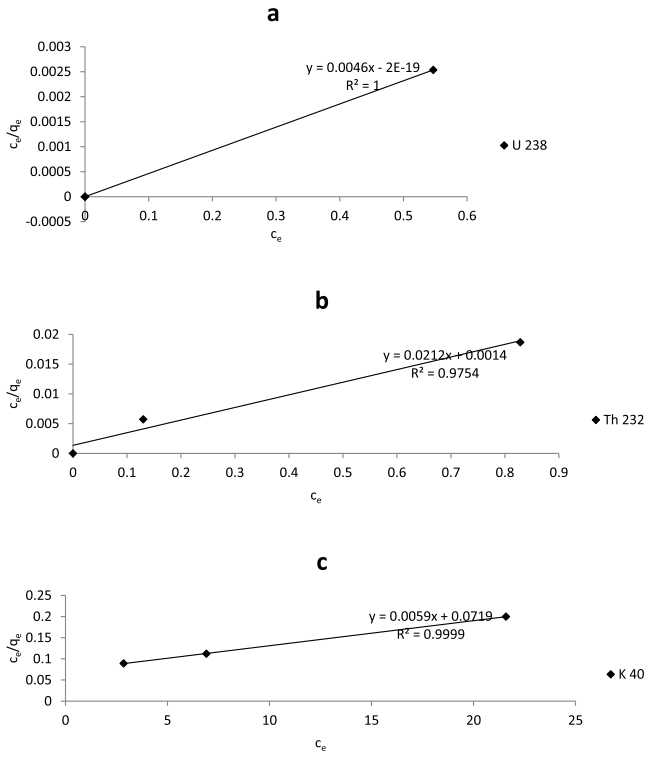

Figure 28. linear Langmuir adsorption isotherms of (a) uranium-238; (b) thorium-232; and (c) potassium-40 onto MWCNTs at 293 K.

adsorption on heterogeneous surfaces, the adsorbent sorption energy drops exponentially when adsorbent sorption sites are saturated. In the linear form, this isotherm is an empirical equation (eq1 12) that can be used to explain heterogeneous systems.[31]

$$\log q_e = \log K_f + \frac{1}{n}\log C_e \tag{12}$$

The adsorption capacity and intensity are represented by the Freundlich constants K_F and $1/n$, respectively. Table 3 presents the values of constants $1/n$ and K_F, which are determined from the slope and intercept, respectively. The plot of log q_e versus log C_e is shown in the results. A value of $1/n$ smaller than 1 indicates good adsorption and validates the heterogeneity of the adsorbent (Figure 29). It also implies that radioactive nuclide ions and MWCNTs have a strong connection (Figure 30).[31]

3.12. D−R Model. Using the D−R isotherm model, which is semi-empirical in nature, the adsorption process is controlled by the pore filling mechanism, assuming multilayer adsorption, van der Waals forces, and physical adsorption processes.[30,31] The linear form of the D−R isotherm model is represented as eq 13

$$\ln q_e = \ln q_s - K_{ad}\varepsilon^2 \tag{13}$$

where q_s is the theoretical isotherm saturation capacity (mg/g), K_{ad} is the D−R isotherm constant (mol^2/J^2), and ε is the Polanyi potential, which is equal to RT ln(1 + 1/C_e), where R (J/mol K) is the gas constant and T(K) is the absolute temperature. Figure 31 shows a linear relation between ln q_e and ε^2. The slope of the plot gives K_{ad} (mol^2/J^2), and the intercept yields the sorption capacity q_s (mg/g) (Table 3). The constant K_{ad} gives an idea about the mean free energy E (kJ/mol) for adsorption per molecule of the adsorbate when it is transferred to the surface of the solid from infinity in the

Table 3. Adsorption Isotherm Constants for the Adsorption of Uranium-238, Thorium-232, and Potassium-40 onto MWCNTs at 293 K

(a) uranium-238											
	Langmuir				Freundlich			Dubinin−Radushkevich			
C° (Bq/L)	q_{max} (mg/g)	b (dm^3/mg)	R^2	R_L	$1/n$	K_f	R^2	ε	K_{ad}	E (kJ/mol)	R^2
111.6				0.66				185.9			
				0.80							
55.80	-2×10^{-19}	0.005	1.0	0.89	−1.71	1.88	0.75	1143.1	2×10^{-8}	1.77×10^{6}	0.01
27.90								0.0			
(b) thorium-232											
	Langmuir				Freundlich			Dubinin−Radushkevich			
C° (Bq/L)	q_{max} (mg/g)	b (dm^3/mg)	R^2	R_L	$1/n$	K_f	R^2	ε	K_{ad}	E (kJ/mol)	R^2
23.57				0.07				541			
				0.80							
11.83	0.001	0.02	0.98	0.89	−0.05	1.34	0.01	4172	5×10^{-9}	5.89×10^{7}	0.01
5.91								0.0			
(c) potassium-40											
	Langmuir				Freundlich			Dubinin−Radushkevich			
C° (Bq/L)	q_{max} (mg/g)	b (dm^3/mg)	R^2	R_L	$1/n$	K_f	R^2	ε	K_{ad}	E (kJ/mol)	R^2
77.22				0.69				732.6			
				0.81							
38.61	0.07	0.01	1.0	0.90	0.60	1.3	0.99	139.2	38×10^{-4}	9.3×10^{1}	1.0
19.30								57.52			

https://doi.org/10.1021/acsomega.2c00819
ACS Omega 2022, 7, 12342−12353

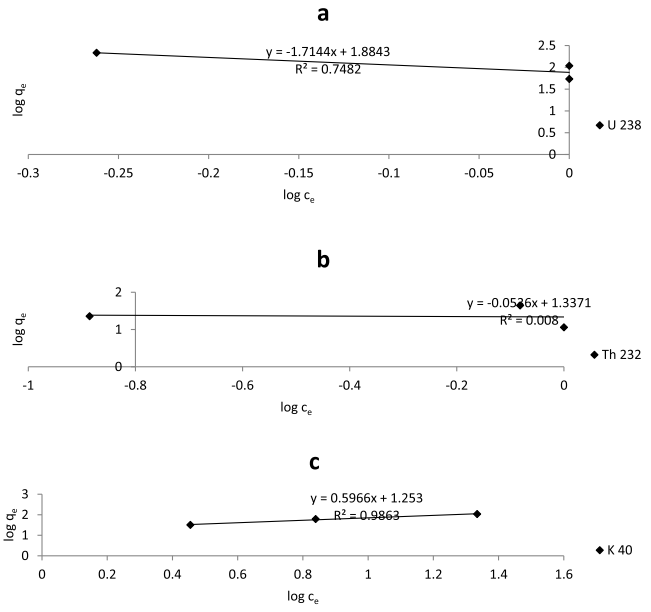

Figure 29. Linear Freundlich adsorption isotherms for (a) uranium-238; (b) thorium-232; and (c) potassium-40 onto MWCNTs at 293 K.

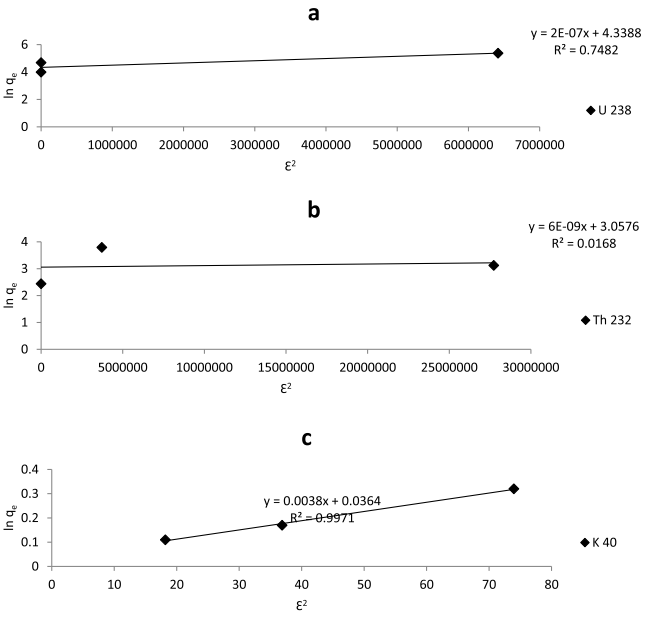

Figure 30. D−R adsorption isotherms of (a) uranium-238, (b) thorium-232, and (c) potassium-40 onto MWCNTs at 293 K.

solution and can be calculated using the relationship given in eq 14.[32]

$$E = 1/(2k_{ad})^{1/2} \quad (14)$$

This value reveals whether chemical ion exchange or physical interaction is the mechanism of metal removal. When E is between 8 and 16 kJ/mol, the adsorption process is referred to as chemical ion exchange, whereas when E is less than 8 kJ/mol, the adsorption process is referred to as physical contact. The adsorption of the mean free energy in uranium-238 is 100 kJ/mol and in thorium-232 is 235 kJ/mol, which corresponds to a physical process.[32] Finally, when the R^2 values

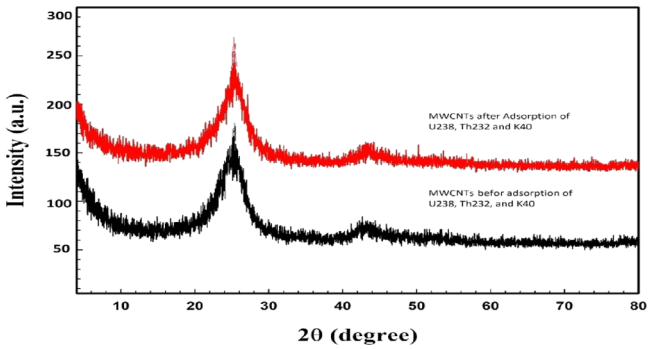

Figure 31. XRD spectra of the MWCNTs before and after adsorption of uranium-238, thorium-232, and potassium-40 metal ions.

in Table 3 are compared, all of the isotherm models fit quite well.

4. X-RAY DIFFRACTION

X-ray diffraction (XRD) spectrometry was conducted in order to clarify whether there is a change in the crystal structure of MWCNTs before and after adsorption. Figure 31 shows that XRD patterns of all MWCNTs before and after adsorption of radionuclides have almost the same first-order diffraction peak at a 2θ of 25.1, which corresponds to a d-spacing of 0.43 nm according to Bragg's equation.[33] This means that adsorption of uranium-238, thorium-232, and potassium-40 leads to no significant change in the crystalline structure of MWCNTs. The main difference in the XRD patterns of MWCNTs is the intensity of the first-order diffraction peak. This difference is probably due to the different adsorption coefficients of the elements present on MWCNTs or due to the transformation of amorphous carbon, leading to an increase of the graphitization degree after adsorption of the radionuclide ions on MWCNTs.[34]

5. CONCLUSIONS

In this study, MWCNTs have been used for the removal of uranium-238, thorium-232, and potassium-40 ions from aqueous solutions. Batch experiments of metal adsorption were carried out to study the effect of pH, contact time, initial metal ion concentration, adsorbent dose, and temperature. Under optimized conditions (contact time = 15 min, pH = 6, and MWCNT concentration = 0.01 mg/L), >98% of uranium-238, thorium-232, and potassium-40 were removed. A pseudo-second-order adsorption model was found to be more suitable for describing the adsorption kinetics. The Langmuir adsorption model displayed the best R_L values for adsorption of uranium-238, thorium-232, and potassium-40 ions in the ranges of 0.66−0.88, 0.06−0.88, and 0.686−0.89, respectively. The Freundlich value of $1/n$ was less than 1, indicating fa avorable adsorption process and confirming the adsorbent's heterogeneity. The thermodynamic data (ΔG, ΔH, and ΔS) reveal an exothermic reaction. No change in the crystal structure of the adsorbate due to the metal adsorption was confirmed via XRD.

AUTHOR INFORMATION

Corresponding Authors

Saad S. M. Hassan − *Chemistry Department, Faculty of Science, Ain Shams University, 11566 Cairo, Egypt*; Email: saadsmhassan@yahoo.com

https://doi.org/10.1021/acsomega.2c00819
ACS Omega 2022, 7, 12342−12353

Ehab M. Abdel Rahman − *Central Laboratory for Environmental Radioactivity Measurements Inter-Comparison and Training (CLERMIT), Nuclear and Radiological Regulatory Authority, 11762 Cairo, Egypt;* orcid.org/0000-0001-9346-9040; Email: Ehababdelrahman@alexu.edu.eg

Authors

Gehan M. El-Subruiti − *Chemistry Department, Faculty of Science, Alexandria University, 45183 Alexandria, Egypt*

Ayman H. Kamel − *Chemistry Department, Faculty of Science, Ain Shams University, 11566 Cairo, Egypt*

Hanan M. Diab − *Central Laboratory for Environmental Radioactivity Measurements Inter-Comparison and Training (CLERMIT), Nuclear and Radiological Regulatory Authority, 11762 Cairo, Egypt*

Complete contact information is available at: https://pubs.acs.org/10.1021/acsomega.2c00819

Notes

The authors declare no competing financial interest.

■ ACKNOWLEDGMENTS

We are deeply thankful for the support of the Central Laboratory for Environmental Radioactivity Measurements Inter-Comparison and Training (CLERMIT), Nuclear and Radiological Regulatory Authority, Cairo, Egypt.

■ REFERENCES

(1) Ojovan, M. I.; Lee, W. E.; Kalmykov, S. N. *An Introduction to Nuclear Waste Immobilisation*, 3rd ed.; Elsevier, 2019.

(2) Al-Khawlany, A.; Khan, A.; Pathan, J. Review on studies in natural background radiation. *Radiat. Protect. Environ.* **2018**, *41*, 215−222.

(3) Oberender, A.; Juel Lyng, R.; Lyngfelt Molander, L.; Jensen, C.; Schouenborg, B.; Theorin, M.; Wærner, E. R.; Røgeberg, M.; Punkkinen, H.; Wahlström, M. *Survey of the Emergence and Use of Naturally Occurring Materials*; Nordic Council of Ministers, 2021.

(4) Labrincha, J.; Puertas, F.; Schroeyers, W.; Kovler, K.; Pontikes, Y.; Nuccetelli, C.; Krivenko, P.; Kovalchuk, O.; Petropavlovsky, O.; Komljenovic, M.; Fidanchevski, E. From NORM by-products to building materials. *Naturally Occurring Radioactive Materials in Construction*; Woodhead Publishing, 2017; pp 183−252.

(5) Nieder, R.; Benbi, D. K.; Reichl, F. X. Health Risks Associated with Radionuclides in Soil Materials. *Soil Components and Human Health*; Springer: Dordrecht, 2018; pp 451−501.

(6) Ojovan, M. I.; Lee, W. E.; Kalmykov, S. N. *An Introduction to Nuclear Waste Immobilisation*; Elsevier, 2019.

(7) Goh, P. S.; Ismail, A. F.; Ng, B. C.; Abdullah, M. S. Recent progresses of forward osmosis membranes formulation and design for wastewater treatment. *Water* **2019**, *11*, 2043.

(8) Madzunya, D.; Dudu, V. P.; Mathuthu, M.; Manjoro, M. Radiological health risk assessment of drinking water and soil dust from Gauteng and North West Provinces, in South Africa. *Heliyon* **2020**, *6*, No. e03392.

(9) Kanwar, V. S.; Sharma, A.; Srivastav, A. L.; Rani, L. Phytoremediation of toxic metals present in soil and water environment: a critical review. *Environ. Sci. Pollut. Res.* **2020**, *27*, 44835.

(10) Bassyouni, M.; Mansi, A. E.; Elgabry, A.; Ibrahim, B. A.; Kassem, O. A.; Alhebeshy, R. Utilization of carbon nanotubes in removal of heavy metals from wastewater: a review of the CNTs' potential and current challenges. *Appl. Phys. A* **2020**, *126*, 38.

(11) Bîru, E. I.; Iovu, H. Graphene Nanocomposites Studied by Raman Spectroscopy. *Raman Spectroscopy*; Federal University of ABC, 2018; p 179.

(12) Kravchenko, J.; Lyerly, H. K. The impact of coal-powered electrical plants and coal ash impoundments on the health of residential communities. *N. C. Med. J.* **2018**, *79*, 289−300.

(13) Abu Samah, N.; Mat Rosli, N. A.; Abdul Manap, A. H.; Abdul Aziz, Y. F.; Mohd Yusoff, M. Synthesis & characterization of ion imprinted polymer for arsenic removal from water: a value addition to the groundwater resources. *Chem. Eng. J.* **2020**, *394*, 124900.

(14) Upadhyay, U.; Sreedhar, I.; Singh, S. A.; Patel, C. M.; Anitha, K. L. Recent advances in heavy metal removal by chitosan based adsorbents. *Carbohydr. Polym.* **2021**, *251*, 117000.

(15) Afkhami, A.; Saber-Tehrani, M.; Bagheri, H. Simultaneous removal of heavy-metal ions in wastewater samples using nano-alumina modified with 2, 4-dinitrophenylhydrazine. *J. Hazard Mater.* **2010**, *181*, 836.

(16) Zheng, H.; Gao, Y.; Zhu, K.; Wang, Q.; Wakeel, M.; Wahid, A.; Alharbi, N. S.; Chen, C. Investigation of the adsorption mechanisms of Pb (II) and 1-naphthol by *β*-cyclodextrin modified graphene oxide nanosheets from aqueous solution. *J. Colloid Interface Sci.* **2018**, *530*, 154−162.

(17) Bhatti, H. N.; Hamid, S. Removal of uranium (VI) from aqueous solutions using Eucalyptus citriodora distillation sludge. *Int. J. Environ. Sci. Technol.* **2014**, *11*, 813−822.

(18) Abdel Rahman, E. M.; Hassan, S. S. M.; Kamel, A. H.; El-Subruiti, G. M.; Diab, H. M. Removal of Uranium-238 Ions from Contaminated Ground Water Containing NORM by Adsorption on Fly Ash Carbon: Equilibrium, Kinetic and Thermodynamic Studies. *Arab J. Nucl. Phys. Material Sci. Appl.* **2021**, *54*, 92−103.

(19) Naseem, Z.; Bhatti, H. N.; Sadaf, S.; Noreen, S.; Ilyas, S. Sorption of uranium (VI) by Trapa bispinosa from aqueous solution: effect of pretreatments and modeling studies. *Desalination Water Treat.* **2016**, *57*, 11121−11132.

(20) Elkady, M.; Shokry, H.; El-Sharkawy, A.; El-Subruiti, G.; Hamad, H. New insights into the activity of green supported nanoscale zero-valent iron composites for enhanced acid blue-25 dye synergistic decolorization from aqueous medium. *J. Mol. Liq.* **2019**, *294*, 111628.

(21) Xie, Y.; Chen, C.; Ren, X.; Wang, X.; Wang, H.; Wang, X. Emerging natural and tailored materials for uranium-contaminated water treatment and environmental remediation. *Prog. Mater. Sci.* **2019**, *103*, 180−234.

(22) Mustafa, J.; Kausar, A.; Bhatti, H. N.; Ilyas, S. Sequestering of uranium (VI) onto eucalyptus bark: kinetic, equilibrium and thermodynamic studies. *Desalination Water Treat.* **2016**, *57*, 14578−14589.

(23) Chauhan, G.; Jadhao, P. R.; Pant, K. K.; Nigam, K. D. P. Novel technologies and conventional processes for recovery of metals from waste electrical and electronic equipment: challenges & opportunities−a review. *J. Environ. Chem. Eng.* **2018**, *6*, 1288−1304.

(24) Younes, A.; Ali, J. S.; Duda, A.; Alliot, C.; Huclier-Markai, S.; Wang, J.; Kabalan, F.; Nemirovsky, D.; Deng, R.; Nur, M. T.; Cao, M.; Groveman, S.; Drain, C. M.; Alexandratos, S. D. Uptake and Removal of Uranium by and from Human Teeth. *Chem. Res. Toxicol.* **2021**, *34*, 880−891.

(25) Azizian, S. Kinetic models of sorption: a theoretical analysis. *J. Colloid Interface Sci.* **2004**, *276*, 47−52.

(26) Khalil, M. A.; El-Kady, M. F.; El-Subruiti, G. M.; El-Sayed, E. M. Influence of natural and synthetic blended polymers on the electrospun PVA/chitosan/PANI composite nanofibers to be used for dye decolorization. *Desalin. Water Treat.* **2020**, *181*, 436−446.

(27) Ghaedi, M.; Tashkhourian, J.; Pebdani, A. A.; Sadeghian, B.; Ana, F. N. Equilibrium, kinetic and thermodynamic study of removal of reactive orange 12 on platinum nanoparticle loaded on activated carbon as novel adsorbent. *Korean J. Chem. Eng.* **2011**, *28*, 2255−2261.

(28) Singh, H.; Javadpour, F. Langmuir slip-Langmuir sorption permeability model of shale. *Fuel* **2016**, *164*, 28−37.

(29) Munagapati, V. S.; Kim, D.-S. Equilibrium isotherms, kinetics, and thermodynamics studies for congo red adsorption using calcium

alginate beads impregnated with nano-goethite. *Ecotoxicol. Environ. Saf.* **2017**, *141*, 226−234.
(30) Ho, Y.-S.; Chiu, W.-T.; Wang, C.-C. Regression analysis for the sorption isotherms of basic dyes on sugarcane dust. *Bioresour. Technol.* **2005**, *96*, 1285−1291.
(31) Feng, C. Removal of Arsenic from Alkaline Process Water of Gold Cyanidation by Use of Functionalised Magnetic Adsorbents, Curtin Theses; Curtin University, 2017.
(32) Junejo, R.; Jalbani, N. S.; Memon, S.; Kaya, S.; Erkan, S.; Serdaroğlu, G.; Palabiyik, I. M. Equilibrium, Thermodynamic, and Density Functional Theory Modeling Studies for the Removal of Dichromate Ions from Wastewater Using Calix (4) arene Modified Silica Resin. *J. Chem. Eng. Data* **2020**, *66*, 379−388.
(33) Bounakhla, M.; Tahri, M. *X-ray Fluorescence Analytical Techniques*; National Center for Energy Sciences and Nuclear Techniques (CNESTEN): Rabat, Morocco, 2014; Vol. *1*; pp 1−73.
(34) Tian, Q.; Sasaki, K. Application of fly ash-based materials for stabilization/solidification of cesium and strontium. *Environ. Sci. Pollut. Res.* **2019**, *26*, 23542−23554.

https://doi.org/10.1021/acsomega.2c00819
ACS Omega 2022, 7, 12342−12353